On Error Analysis of High Data Rate, Optical Parallel Processors

Deborah J. Jackson

Jet Propulsion Laboratory

California Institute of Technology

Pasadena CA 91109

Mario L. Juncosa

RAND Corporation

Santa Monica CA 90407

Abstract

Optical parallel processors have the potential for aiding the transfer of information over networks. This exploratory study examines the systems implications for a baseline architecture employing spatial light modulators (SLM), lenses, and charged coupled devices (CCD). Specifically, this study categorizes potential error sources — both random and systematic error sources — and presents the results of an error analysis for a pixel-to-pixel mapping system.

On Error Analysis of High Data Rate, Optical Parallel Processors

1.0 Introduction

Recent advances have led to faster, more reliable spatial light modulators (SLM), thereby opening up the possibility of achieving real-time processing at high data rates via space division multiplexing (SDM) in photonic architectures. Possibilities may include the use of SLMs in tandem. Several general classes of applications can benefit from such an architecture. For example:

- High-speed optical routers.
- high speed optical encryption.

Figure 1 illustrates a baseline architecture that is useful in evaluating the random bit error rate (BER) issues for both application areas. In fact, the general purpose of this paper is to classify and examine both random and systematic error sources and to present formulas for their quantification. In all cases, the input and output configurations at SLM_1 and CCD_1 are the same. In addition, SLM_1 and CCD_1 are also assumed to have identical $N \times N$ array sizes and pixel pitches, such that one-to-one mapping takes place from input to output.

Incidentally, we also note here the option of storing an n-ary character in each pixel — instead of using a 1-bit character —to further increase the throughput rate. Thus, a high-rate input-data stream is fanned out into a two-dimensional image format, as is shown in Figure 2.

In image format, each bit is read into the SLM array pixel by pixel, line by line. The bit sequence read into the jk^{th} pixel determines the SLM phase, δ_{jk}, such that the spatial phase variation or the readout from the SLM contains the reformatted digital input word.

Assuming an input data rate $DR_{input} \geq 40$ Gbps, fanning the data stream out into a two-dimensional array for processing permits one to slow the clock rate down at SLM_2. This tactic can be used to accommodate the intrinsically slower device speeds of the less mature SLM devices. The SLM_2 clock rate, CLK, is governed by the data rate of the input data stream, the array size, and the grayscale index at the pixel level. Hence, the slowest possible clock rate permissible at SLM_2 is

$$CLK = \frac{DR_{input}}{NxNxn}. \qquad \text{Equation 1}$$

Of course, this relationship holds true only if a single parallel operation is required at SLM_2 to permute or encrypt the full input frame. If more than one operation is required, the minimum clock rate is actually

$$CLK_{\min} = \frac{DR_{input}}{NxNxn} \#OPS, \qquad \text{Equation 2}$$

where #OPS is the number of logic operations performed in parallel.

At SLM_2, the optical-processing modulation input varies with each application. For example, in the high-data-rate optical-router application, each row in SLM_1 is loaded with packets arriving in parallel for different destinations, as designated by the packet's header. SLM_2, therefore, is loaded with a hologram that permutes the order of the rows initially loaded into SLM_1 to a different order at the CCD_1 output. In the encryption application, the phase information loaded into SLM_1 is scrambled by adding random phase to each pixel at SLM_2. Such an encryption architecture permits the use of extremely large encryption keys.

Each application has very different BER requirements that must be met for a single stage of the baseline configuration, as is shown, for example, in Table 1. Moreover, for both of the cited application examples, the more interesting problems can be addressed by cascading multiple stages of the baseline configuration[1]. Consequently,

it is important to determine how much information is lost or corrupted each time one passes through the baseline stage.

2.0 Error Analysis

An error is defined as an instance where one character is mistaken for another (for example, 1 for 0). For applications such as transmitting cryptotext, numerical-valued data, or similar material that has little or no redundancy, clearly, the systems employed — optical and otherwise — must have extremely low tolerances for error. Errors fall into two classes: *random errors* or *statistical* errors; i.e., noise and systematic, or bias, errors. For a successful system design, a careful error analysis — such as the one that follows — is a prerequisite.

2.1 Random Errors

Random errors, which can have several causes, are not individually predictable; instead, random errors can be predicted statistically at some level of confidence and are usually quantified by the variances of their particular probability distributions.

Considering the flow as photonic, the distribution of the flow and of the accompanying errors is Poisson; however, for large Poisson parameter values or errors in the intensity flow, the Gaussian (normal) distribution probably suffices. Thus, the random errors are measured as bit error rates (BER), which are actually the probabilities of error (POE) of encountering a misrepresented bit or character. These POEs are the extreme tails of normal distributions whose variances are determined by the noise levels.

The BERs or POEs are obtained from basic statistical decision procedures. Although BERs and POEs are general, we consider for a definite example the case where the distribution is Gaussian (see. Figure 3). To begin with, we illustrate the binary decision case; i.e., a 1-bit grayscale level with two possible signals: 0 and 1. With 0 the

mean of one probability distribution and 1 the mean of the other distribution, the respective probability densities overlap. A decision point, D, is chosen such that

- If an observed sample falls to the left of D, the decision calls for the signal to be classified as a 0.
- If an observed sample falls to the right of D, then the signal is to be classified as a 1.

However, because some of the "0" probability density falls on the "1" side of the decision point, and vice versa, there is a small possibility that a zero bit will be erroneously read as a one, and vice versa. The POE used for this determination is, thus

$$POE = \frac{1}{\sqrt{2\pi}}\int_{Q_0}^{\infty} \exp\left(-\frac{x^2}{2}\right)dx + \frac{1}{\sqrt{2\pi}}\int_{-\infty}^{Q_1} \exp\left(-\frac{x^2}{2}\right)dx \qquad \text{Equation 3}$$

where

$$Q_i = \frac{D - s_i}{\sigma_i};\ \ i = 0,1 \qquad \text{Equation 4}$$

s_1 (s_0) is the expected value of the signal associated with a 1 (0), σ_1 (σ_0) is its standard deviation, and D is the decision point set by the optical receiver in the imaging plane. The decision point is equal to $(s_0 + s_1)/2$ when the standard deviations, σ_i, are equal. When the standard deviations are unequal, then D is chosen so as to make the areas of the two tails in Equation 3 equal.

In a situation where each pixel is used to detect an n-bit grayscale, Equation 1 must be generalized to the following

$$POE_{n-bit} = \sum_{i=1}^{2^n-1}\left[\frac{1}{\sqrt{2\pi}}\int_{a_i}^{\infty} \exp\left(-\frac{x^2}{2}\right)dx + \frac{1}{\sqrt{2\pi}}\int_{-\infty}^{b_i} \exp\left(-\frac{x^2}{2}\right)dx\right] \qquad \text{Equation 5}$$

where

$$a_i \equiv Q_{i-1} = \frac{D_{i-1} - s_{i-1}}{\sigma_{i-1}}, \quad b_i \equiv Q_i' = \frac{D_{i-1} - s_i}{\sigma_i}, \quad s_i = \frac{s_{(2^n-1)}}{(2^n - 1)} \cdot i \qquad \text{Equation 6}$$

and D_i is chosen following the same rules mentioned above in the case where n = 1. We ignore the infinitesimal probability of mistaking the nonadjacent grayscale values.

If there is an n-bit grayscale level and the error probability distributions associated with the different gray levels differ only in their mean values, this expression is simplified to

$$POE_{n-bit} = (2^n - 1)\left[\frac{1}{\sqrt{2\pi}}\int_{a_i}^{\infty} \exp\left(-\frac{x^2}{2}\right)dx + \frac{1}{\sqrt{2\pi}}\int_{-\infty}^{b_i} \exp\left(-\frac{x^2}{2}\right)dx\right]. \qquad \text{Equation 7}$$

This equation demonstrates that going to a higher grayscale always increases the POE. Furthermore, the detection at the CCD is not linear in the phase; therefore, the probability distribution varies from level to level within the grayscale. Thus, once n is selected, the distribution and decision points should be customized for each level.

The same error sources show up after transmission and decryption of the message. Thus, the anticipated probability of error for a complete encryption/decryption cycle is:

$$POE_{encrypt+decrypt} = 2(POE_{n-bit}). \qquad \text{Equation 8}$$

This assumes that the chosen transmission protocol permits essentially "perfect" transmission over the network; therefore, that segment can be ignored.

Because the most commonly encountered graphs for POEs run up to a limit of 10^{-10}, with the aid of some probability tables dating back to the 1940s[2], we extended the graph up to a limit of 10^{-44} (see Figure 4).

The characteristic figure of merit for most systems transmitting or emitting something is the signal-to-noise level, S/N, at the receiver. Thus, here one needs a measure of the intensity of light at the receiver and the intensity of the noise from all sources, equipment as well as environment.

The principal random noise contributions are: thermal noise, shot noise, relative intensity noise (RIN), and noise internal to the SLMs themselves. For a single detector, the ratio of the total received photocurrent, I_0, one must be able to detect the intensity associated with the minimum phase increment $I_{\min} = I_0 \sin[\pi/2(2^n - 1)]$ with good signal to noise. The ratio of the minimum signal to the noise due to the first three noises at the imager is given by[3]

$$\frac{S}{N} = \frac{(I_{\min} m)^2}{2B\left[n_e^2 + I_{\min}^2\left\{\frac{2e}{I_{\min}} + RIN\right\}\right]}, \qquad \text{Equation 9}$$

where B is the bandwidth, $n_e^2 = 4kT/R_l$ is the preamplifier-equivalent input-noise current, k is Boltzman's constant, T is the ambient absolute temperature, R_l is the input impedance of the preamplifier, e is the electric charge, and m is the modulation depth. In the special case when n = 1, we find that $I_{\min}$ simplifies to I_0. The first term in the denominator is the thermal noise contribution from the resistance at the preamplifier input.

The second term in the denominator is the contribution from the shot noise. The third term in the denominator is due to the relative intensity noise (RIN or amplitude fluctuations of the laser.

Generally, for CCD detector arrays, the noise is determined by the thermal noise of the amplifier circuit; therefore, no attention is paid to noise variations due to the light source. However, the second and third terms become much more important for our application where the absolute intensity of the light source is needed to discern the phase angle upon capture at the CCD. Because both spatial and temporal variations effect the bit error rate, controlling these variations becomes a significant concern in this application.

Assuming that stray light is at levels considerably below the noise from the above sources and that there are no correlations between the different noise sources, we have for the variance of the total noise[3]

$$\sigma_i^2 = \frac{8kTB}{R_i} + 4eBI_{\min} + 2BI_{\min}^2(RIN) + \sigma_{SLM}^2 , \qquad \text{Equation 10}$$

There has not been an extensive history of error modeling and verification with the SLM. Consequently, the Gaussian or approximately Gaussian nature of the SLM noise sources needs to be verified before it can be assumed in Equation 13. The distribution of error due to the SLM itself may not be Gaussian. Consequently, the total variance would not be a variance associated with a Gaussian distribution. If the SLM error distribution were Gaussian or approximately Gaussian, the total variance above would also be so and the POEs — or, equivalently, the BERs — can be determined by Equation 13. If the SLM is well behaved (that is, the SLM's noise variance is negligible compared to the shot noise, thermal noise, and laser noise terms), we can calculate representative numbers for the error probabilities due to random noise sources. The

representative numbers are inferred from the values of Q calculated in Table 2 as a function of the n-bit grayscale level using the following expression

$$\sigma_i^2 = \frac{8kTB}{R_t} + 4eBI_{\min} + 2BI_{\min}^2(RIN). \qquad \text{Equation 11}$$

The results in Table 2 are based on the following assumptions:

- 100,000 frames/second throughput rate.
- 12.8 MHz line rate.
- 128 × 128 readout CCD array.
- 200,000 electrons/pixel well-depths, representing a line current, $I_0 = 0.41$ μAmps.
- Bandwidth = 108 MHz.
- RIN = -160 dBc/Hz
- Thermal, shot, and RIN noise distributions are Gaussian or approximately so.
- SLM random noise is much less than the shot-noise term.
- Measurements taken in the linear part of the curve*.

*This assumption implies that the discretization discussed in Section 3.4 is achieved by having adjacent rows contain the same phase information, but offset by $\pi/4$ so that one row or the other will always yield intensity values from the linear part of the curve.

In Table 2, the Q is calculated by assuming that the SLM noise contribution in Equation 13 is negligible. Clearly, when n = 1 and the maximum line current is 0.41 μAmps, the noise is dominated by the photon statistics of the shot noise term. With a Q of roughly 77, the probability of misreading a bit is negligibly small. Of course, as one goes to finer and finer grayscales, the random noise contribution to the least significant bit increases because the information in each bit is conveyed by fewer and fewer electrons. However, even a 7-bit grayscale provides a POE or anticipated BER of 10^{-8}. Again this implies that there is a large trade space for designing the hardware for this application. The above treatment assumes that all the noise-source contributions in Equation 13 are approximately Gaussian in behavior. However, the liquid crystal SLMs that have been characterized in the literature thus far do not adhere to this ideal behavior.

The only data we found were three liquid crystal SLM designs in a 1995 thesis by Morelli.[4]. Morelli's results show graphs with distinctly non-Gaussian characteristics, which he attempted to model by developing empirical fits to the data. Some graphs show a nearly periodic behavior superposed with noise; others graphs show unusual jumps superposed with noise. Morelli conjectures[5] that the non-Gaussian characteristics may be due to some internal transitions in the liquid crystals under the influence of external fields; as deterministic phenomena, these transitions may be removed through calibration leaving the random noise component.

If this remaining component is Gaussian (and reasonably assumed to be uncorrelated with the others), then its variance can be incorporated with the others to give a total noise that would be Gaussian. If the remaining component is not Gaussian but quite small in variance when compared to the other noise sources, then it may be ignored. If the remaining component is large in variance compared to the thermal noise, shot noise, and RIN noise, those noise terms can be ignored. Consequently, one is left with determining an accurate empirical distribution to measure tails on the error terms well enough to get a POE or BER that is credible – a decidedly difficult task. If the SLM's residual random error component is comparable to the total variance of the other noise terms, then a convolution of a Gaussian with some non-Gaussian empirical distribution must be obtained with sufficient accuracy in the tails to produce credible POEs or BERs. Again, because of the stringent BER demands this task is expected to be difficult.

It should be emphasized that the recent developments of micro-electromechanical devices (MEMS) SLMs may offer the possibility of observing more Gaussian-like distributions in the SLM noise variance. It is clearly critical that an analysis of the noise characteristics of MEMS SLMs or any others that may develop be carefully determined to be Gaussian before casually using Equation 13 to add to the thermal noise, shot noise, and RIN noise components of the total noise distribution variance.

2.2 Systematic Error Sources

Lens characteristics and the relation of the lenses to the SLMs are the main source of systematic error. Some of the systematic error is likely to be removed by calibration. Among the potential sources for systematic error are propagation losses due to the finite lens diameter relative to the active fields of the SLMs.

A concern is that information can be truncated by the lens pupil. Other concerns include spherical aberrations due to the lenses, interaction between spherical aberration and the fill factors of the SLMs, and truncating effects of aperture stops.

2.2.1 Truncating Effects of Lens Pupil Size

The pixel-to-pixel mapping case is treated in Appendix A, where we derive a formula for the maximum SLM diagonal, d_{max}, such that a marginal ray from a corner of a hypothetical SLM would touch the lens diameter (pupil), D, refract, and reach a second identical SLM at the same corner. Figure A.1 of Appendix A illustrates this pixel-to-pixel mapping. Clearly, any rays emanating from the first SLM above the marginal ray would not intersect the lens. Moreover, the marginal ray does not image the first SLM's pixel onto its proper pixel at the second SLM. The only rays that are imaged are rays nearly parallel to the optical axis. Additionally, rays passing through the center of the lens would image in focus. Therefore, the marginal calculation is conservatively yielding a substantially larger diameter than required for the pixel-to-pixel operation. We assume a symmetric doubly convex lens with diameter D, a radius of curvature R, and an index of refraction n. Appendix A contains the derivation of d_{max}. The result is

$$d_{\max} = D\left\{1 - \frac{\left[n\left(\left(1-n^2D^2\right)/4R^2\right)^{\frac{1}{2}} - \left(1-D^2/4R^2\right)\right]}{(n-1)\left[1-\left(n^2+1\right)D^2/4R^2\right]}\right\}. \qquad \text{Equation 12}$$

For example, if R = 15 cm, D = 3 cm, and n = 1.6, the calculated value for d_{max} is 1.432 cm. For an SLM of 256 × 256 pixels and a pitch of 20 μ (or 0.002 cm), the diagonal length of active field is 0.724 cm (slightly more than half of d_{max}).

Considering the SLM as an aperture, there is a rapid intensity fall off from the normal. Therefore, for relative dimensions approximately the same as these, we can expect no influence of lens pupil size at the image plane. (This analysis is based on standard Fraunhofer diffraction theory assumptions that appear in texts such as Born and Wolf[6].)

Although the derivations for the plano-convex lenses are much more algebraically complex than the symmetric doubly convex cases, one can expect similar results for similar optical component parameters.

2.2.2 Spherical Aberration Considerations

Again we examined a pixel-to-pixel mapping situation with spherical doubly convex lenses or with plano-spherically convex lenses with light rays incident on either side of the lens. (Figures B.1, B.2, and B.3 in Appendix B illustrate this example.) In particular, we were concerned with determining the errors of displacement transverse to the optical axis due to spherical aberration, which could cause spillover to neighboring pixels at the target SLM or CCD if sufficiently great. Formulas are derived for the rays emerging from the lens and focused toward the target SLM or CCD. The rays, or course, are considered parallel to the optical axis before entering the lens. The geometrical optics, algebra, and trigonometric manipulations are used to arrive at the derivations and formulas are detailed in Appendix B.

We considered the pixel of the originating ray to be at one of the four corners of the SLM because the greatest transverse displacement error would be expected for the ray at the focus and at the image plane. The off-axis deviations at two points — at the lens focus and at twice the focal length distance — were calculated for the cases of each lens situation.

We assumed SLM of 256 × 256 pixels with a pitch of 20 microns (or 0.002 cm), a radius of curvature of 15 cm for the spherical faces of the lenses and a diameter of the lens of 3 cm for all three cases. The results of our calculations are summarized in Table 3. Using a thick lens formula for the focal length would make very little difference in these results.

What are the implications of the results in Table 3 for lens and SLM parameter choices? Assuming pixel-to-pixel mapping with similar parameters for the SLMs as for the CCDs:

- In case (a) of our example, the size of the transverse aberrations is unacceptable because of significant spillover to neighboring CCD pixels. The spillover is enough to make possible a distinct error (even in the case of a simple binary grayscale).
- For case (b), if the grayscale levels do not exceed four, the results are acceptable for application. At eight grayscale levels, the results would be marginal.
- For case (c), an n = 2 grayscale index would be the most one would accept for applications.

The fill factors of the SLM have some interaction with the aberration in affecting the results; the interaction between fill factors and aberrations will be discussed below. However, these cases indicate that aberrational effects are not negligible. Consequently, care in selecting the physical parameters of all optical elements is important.

The errors produced by observations due to the spherical lens can be controlled by several means, including:

- Careful selection of lens radius of curvature and/or diameter.

- Use of commercial lens designed to remove aberration.
- Adjusting the size of the fill factor to diminish aberration-induced transverse spillover.
- Controlling the half diagonal dimension of the SLM and CCD.

2.2.3 Fill-Factor Considerations

The fill factor of an SLM or CCD is the square of the ratio of the pixel width to the pitch, thereby determining the fraction of the SLM face that is active. Because we are re-imaging from SLM_1 to SLM_2 and from SLM_2 to CCD_1 in the pixel-to-pixel configuration, the size of the fill factors can be chosen to cancel out any transverse spillovers to neighboring pixels in the target SLM. Therefore, the fill factor can be used to correct for the previously discussed transverse deviations caused by spherical aberrations of the lenses. There is clearly a trade-off between optimizing the active pixel area to optimize the signal intensity recovered at the pixel and reducing the fill factor to cancel the transverse spillover. As one goes to higher grayscale levels, absolute intensity becomes important in achieving good photon statistics, such that the spillover trade-off is much less desirable. In this situation, increasing the radius of curvature of the lens can be used to decrease the transverse aberration.

To examine the effects of the interactions between aberration-induced spillover and fill factors of SLMs (see Figure 5), we treat the simplest case: a case that assumes that the SLMs and the CCDs have the same pixel number and pitch lengths and that the CCDs have 100% fill factors. For SLM 100% fill factors, there is significant loss due to the transverse spillover effect. However, as the fill factor decreases, the loss due to the transverse aberration continues, but the amount of spillover into adjacent pixels is reduced because some or all of the spillover falls into the inactive area of the pixel.

The design optimization comes from using Equation 17 and Equation 18 to determine the smallest active area that yields an acceptable capture of photon statistics with minimum crosstalk among the pixels.

A combination of adjusting the fill factor and carefully selecting the radii of curvature on the lens can be used to minimize spillover into adjacent pixels. In Figure 5, four pixels of a 100% fill factor CCD are represented, the lower left being the intended recipient of the information from a pixel of an SLM with a fill factor denoted by f. Both the SLM and the CCD have a pitch denoted by p. In the absence of aberration, regardless of the fill factor of the SLM, all information from the SLM pixel is captured by the intended target CCD pixel. The translation of the pixel under aberration due to the intervening lens the center of the SLM's pixel information is given by coordinates (t_b, t_a) at the plane of the CCD (indicated by an arrow in Figure 5). Therefore, the area of the transformed pixel that overlaps with its target CCD pixel is given by

$$ab = \left(p - |t_a|\right)\left(p - |t_b|\right). \qquad \text{Equation 13}$$

With a fill factor of f < 100% on the SLM, the amount of the original active area captured on the intended target pixel at the CCD is

$$\left[a - (p/2)\left(1 - f^{\frac{1}{2}}\right)\right]\left[b - (p/2)\left(1 - f^{\frac{1}{2}}\right)\right] = ab - (a+b)(p/2)\left(1 - f^{\frac{1}{2}}\right) + (p/2)\left(1 - f^{\frac{1}{2}}\right)^2.$$

Equation 14

Consequently, the ratio of active area capture on the target to the amount the CCD pixel would have captured with an SLM fill factor of 100% is then

$$1 - (1/ab)\left[(a+b)^2 - \left(a + b - p/2\left(1 - f^{\frac{1}{2}}\right)\right)^2\right]. \qquad \text{Equation 15}$$

This is clearly an increasing function of f; i. e., the greater f is, the greater the ratio becomes until f = 1 when the ratio becomes 1.

In the other direction, the ratio becomes zero not when f reaches zero, but, instead, at a positive value, the greater of the two

$$\left[1-2\left((a+b)+\frac{\left((a+b)^2-ab\right)^{\frac{1}{2}}}{p}\right)\right] \text{ or } \left[1-2\left((a+b)-\frac{\left((a+b)^2-ab\right)^{\frac{1}{2}}}{p}\right)\right].$$

Equation 16

The choice between these equations is dependent on the relative sizes of p and $2(a+b)$, the quantity with the positive sign before the square root if $2(a+b) > p$ and the quantity with the negative sign before the square root.

On the other hand, one can make a contrasting observation. Specifically, for modest displacements due to aberration displacements (less than a pixel length), one may require decreased fill factors to avoid information spillover (cross-talk) to pixels at the CCD that are neighbors of the intended target pixel. Taking Figure 5 to illustrate the point, we note that, for no spillover, the SLM's inactive border must be broad enough that no part of the active area arriving at the CCD crosses the boundary of the intended receiving CCD pixel. Clearly, for there to be any active area at all, both a and b must be greater than p/2; however, for definiteness with no loss in generality, let us assume that $p/2 < a < b$. For no spillover to the upper left CCD pixel, the top border of the SLM pixel's inactive area must be at least $p-a$ wide. With a conventional equal width inactive border on all sides of the active area, the maximum active area without spillover is then $\left(p-2(p-a)\right)^2 = (2a-p)^2$. Such an active area implies a fill factor of $(2a-p)^2/p^2 = (2a/p-1)^2$, which, in the presence of aberration, is less than 100%.

With vertical components of the aberration-caused transverse displacement of the SLM pixel's image at the CCD of 0.1 p, 0.2 p, and 0.3 p, a = 0.9 p, 0.8 p, and 0.7 p, respectively, and resulting maximum fill factors of 64%, 36%, and 16%, respectively, we get no spillovers of active information to neighboring CCD pixels.

Therefore, we conclude the following: in the light of the observations detailed above and considering the earlier numerical results regarding acceptability or non-acceptability of certain aberration distances (depending on the number of grayscale levels), the choice of parameters of elements in the design of an SLMs-lenses-CCD system for pixel-to-pixel mapping requires simultaneous consideration of several interacting factors. The choices can not be made considering each factor independent of the others.

2.2.4 Aperture Stops and Stray Light Control Considerations

In this section, stops are considered not as a source of error, but, instead, as one of the agents used to control error. An aperture stop could be used to facilitate incoherent-stray-light control. Placing an aperture stop between a lens plane and its image plane is particularly effective. The SLMs and CCDs considered are assumed to be square in their pixel field shape. The intent of this analysis is to determine the dimensions of a minimum admissible square aperture and the location of the stop. The findings are based on standard thin-lens ray-optics procedures that locate points on the image plane corresponding to points in the object plane in an aberration-free situation. The objects in the object and image planes can be SLMs, CCDs, or other optical objects.

Figure 6 (which is not to scale) illustrates the setup in the analysis. In Figure 6, a stop is placed between the lens plane and image plane and is parallel to them. The SLMs, CCDs, and stops are centered on the lens' optical axis. The standard procedure for image-point locations is to follow two rays from an object point to their coincidence at the image plane. This is illustrated in Figure 6 by the pair of rays from P_1: one ray passes through refraction at O_1 and then on through the focus F to Q_1, the other ray passes through O, the center of the lens, and then on to Q_1. The two rays from P_2 ($P_2O_2Q_2$ and P_2OQ_2) illustrate the same procedure. The length of the segment P_1P_2 is h, the height of a side of the object SLM or CCD. Similarly, if p and q are the respective object and image distances from O (the center of the lens), the length of the segment Q_1Q_2 is hq/p, the height of a side of the corresponding image.

Our goal is for the intersection (y_a, z_a) of the ray segments O_1Q_1 and P_2Q_2, y_a to be the half height of the aperture and for z_a to be the location of the stop plane in a rectangular coordinate system with O as the origin. The equation of the line containing the segment O_1Q_1, from a consideration of similar triangles, is

$$y = \frac{h}{2f}(f - z), \qquad \text{Equation 17}$$

where f is the distance from O to the focus F. The equation of the line containing the segment P_2Q_2 is

$$y = \frac{h}{2p}z. \qquad \text{Equation 18}$$

Solving these two equations for the intersection of their two lines, we get

$$y_a = \frac{hf}{2}(p + f) \qquad \text{Equation 19}$$

and

$$z_a = pf(p + f). \qquad \text{Equation 20}$$

Therefore, the minimum aperture is a square that is $hf/(p+f)$ on a side and the stop plane is located at a distance $pf/(p+f)$ from O between the lens plane and the image plane.

In one-to-one pixel mapping, $p = q = 2f$, these results simplify to a square aperture of $h/3$ on a side with the stop placed at a distance $(2/3)f$ from O toward the image plane in the ideal thin lens aberration-free case. Additional stops with similar dimensions can be placed with the additional lenses in the baseline configuration.

Even though the thin lens assumption is acceptable, we assumed an ideal situation; however, aberrations are to be expected. (The analysis quantifying the transverse deviations of the rays was treated in a preceding section and is treated further in Appendix B.) If the aberration-caused deviation errors are within acceptable bounds for any particular case, $2^{1/2}$ times these deviations must be added to the lengths of the sides of the aperture for the stop to be admissible.

3.0 Summary and Conclusions

Systematic errors, which are frequently bias errors or aberration errors for optical components, are caused by a variety of sources. Knowledge of the systematic errors is necessary to calibrate for the potential bias and to filter known perturbing periodicities (if the system possesses any). Ultimately, the objective is to adjust the design or select components so that systematic errors are far enough below the random-error contribution to the total error to be ignored. Table 4 summarizes our findings with respect to the systematic error sources.

It is anticipated that all of the systematic sources are either negligible or can be easily compensated for through calibration. The exception is the contribution from scattered stray light; aperture stops can be used to reduce stray light. The key, therefore, is careful design and quality control of the optical elements.

Random noise contributions are summarized in Equation 13; the analysis depends very closely on the type of SLM chosen and its design details. In the data that currently exists for three different types of liquid crystal SLMs, the noise variance is dominated by noise caused by the SLM. In each case, these SLMs also exhibited enough of a non-Gaussian noise variance that it was clear that detailed empirical fits to the distribution tails would be necessary to give meaning to error probabilities below 10^{-3}. For liquid crystal SLMs, the phase modulation is dependent on electrically induced refractive index changes in the complex liquid crystals. In all likelihood, the complex behavior observed in the variance is also due to higher order interactions of the electronic field with the liquid crystal medium; these interactions limit the precision with which the phase setting can be determined. Morelli has determined that, using the SLMs he tested, useful probabilities of errors would be 10^{-3}. Thus, liquid crystal SLMs would not be useful for the router or encryption applications under consideration here, but could prove very useful in image correlation applications[7] where the information contained in a single pixel is not as important as the relative distribution of information in adjacent pixels.

Such higher-order effects are much less likely to be observable with the recently developed MEMS SLM devices. In fact, there is hope that the noise variance in the MEMS SLMs will not only be Gaussian-like in behavior, but also less than the shot noise contribution. This would permit one to use Equation 13 without reservation; in that instance, BER performance below 10^{-9} could be expected in applications such as high-speed routers, high-data-rate encryption, or cascading operations. The analysis clearly suggests that in the physical limit for the precision of optical computation will be due the shot noise of the optical source. This may have implications for some of the quantum cryptography models that are in the published literature[8].

ACKNOWLEDGEMENTS

The work described in this paper was carried out by the Jet Propulsion Laboratory, California Institute of Technology, and was sponsored by the National Security Agency.

Reference herein to any specific commercial product, process, or service by trade name, trademark, manufacturer, or otherwise, does not constitute or imply its endorsement by the United States Government or the Jet Propulsion Laboratory, California Institute of Technology.

The authors with to thank Dr. Michael Morelli at Sirostech Corporation for clarifying discussions on his thesis relating to liquid crystal SLM noise analyses.

REFERENCES

1. Jackson, D. J.,"Photonic Processors: A Systems Approach", *Applied Optics* Vol. 33, No. 5, 5451-5466 (1994)
2. *Tables of Probability Functions*, Table II, Vol. I, Vol. II, Arnold N. Lowan, Technical Director, Mathematical Tables Project, National Bureau of Standards, 1941, 1942.
3. Darcie, Thomas E. and George E. Bodeep, *Lightwave Subcarrier CATV Transmission Systems,* IEEE Transactions on Microwave Theory and Techniques, Vol. 38, No. 5, May 1990.
4. Morelli, Michael V., *Complex-Amplitude Noise and Accuracy Analysis of Quantized Analog Optical Processors*, Ph.D. Thesis, Optical Systems Laboratory, Department of Electrical Engineering, Texas Tech University, Lubbock, May 1995.
5. Private communication with M. Morrelli.
6. Born, Max and Emil Wolf, *Principles of Optics*, 4th Edition, Pergamon Press, Oxford, 1970, p. 393.
7. A. VanderLugt, "Signal detection by complex spatial filtering" IEEE Transactions on Information Theory, IT-10, 130 - 145 (1964).
8. Gershenfeld, N. and Chuang, I. L., "Quantum Computing with Molecules", *Scientific American*, June 1998; Bennett, C. H., "Quantum Information and Computation", *Physics Today*, Vol. 48, No. 10, October 1995, 24 - 31; Hughes, R. and J. Nordholt, "Quantum Crpytography Takes to the Air", *Physics World*, May 1999, 31 - 35.

APPENDIX A — Relation of Lens Diameter to SLM and CCD Maximal Diagonal Dimensions

Given a symmetric, doubly convex thin lens with radius of curvature, R, for each face, diameter, D, and index of refraction, n, we consider pixel-to-pixel mapping from a square pixel array SLM to an SLM or a CCD of the same active field dimensions whose active field diagonal length is d. To determine whether there are errors introduced at the receiving SLM or CCD due to lens pupil restrictions for the typical anticipated dimensions of our setup, we determine the maximum diagonal dimension of the emitting SLM for a marginal ray passing from the emitting SLM to the receiving SLM or CCD that intersects the lens infinitesimally close to its rim.

From Figure A1, assume a ray originating at P that is displaced from the optical axis but on the object focal plane. This ray intersects the lens at Q, a distance h (<D/2) from the optical axis, passes through the lens parallel to the optical axis, exits the lens again at Q' (also a distance h from the optical axis), and terminates at P' on the image focal plane. (Incidentally, P' is not the image of P)

We later pass to the limiting position, where the intersection approaches the rim of the lens (i.e., as h approaches D/2) to obtain an equation for the marginal ray. Our objective is to calculate the maximum diagonal dimension of the square active field of the SLM. The ray's path is symmetric about the lens plane and parallel to the optical axis for the segment that is inside the lens. R is defined as the radius of curvature of the lens, D is the diameter of the lens, h is the height of Q', B is the angle arcsin(h/R), and A is the angle between the normal to the lens surface at point Q' and the outgoing ray, P'Q'.

Using the symbols indicated in Figure A1, we have for the off-optical-axis distance, w, as a function of the distance, z, from the lens center on the optical axis, the following equation

$$(w - h)/(z - (R^2 - h^2)^{1/2} + (R^2 - D^2/4)^{1/2}) = \tan(A - B) \qquad \text{Equation A 1}$$

or

$$w(z) = h + (z - (R^2 - h^2)^{1/2} + (R^2 - D^2/4)^{1/2}) \tan(A - B). \qquad \text{Equation A 2}$$

With sin B = h/R and Snell's Law of Refraction, sin A = n sin B, we have

$$\tan(A-B) = \frac{h\left[n\left(1-h^2/R^2\right)^{\frac{1}{2}} - \left(1-n^2h^2/R^2\right)^{\frac{1}{2}}\right]}{R\left[\left(1-h^2/R^2\right)^{\frac{1}{2}}\left(1-n^2h^2/R^2\right)^{\frac{1}{2}} + nh^2/R^2\right]}. \qquad \text{Equation A 3}$$

We now pass to the limit $h \rightarrow D/2$ to obtain the limiting value for tan(A – B), as follows

$$\tan(A-B) = \frac{(D/2R)\left[n\left(1-D^2/4R^2\right)^{\frac{1}{2}} - \left(1-n^2D^2/4R^2\right)^{\frac{1}{2}}\right]}{\left[\left(1-D^2/4R^2\right)^{\frac{1}{2}}\left(1-n^2D^2/4R^2\right)^{\frac{1}{2}} + nD^2/4R^2\right]}$$

$$= \frac{(D/2R)\left[n\left(1-n^2D^2/4R^2\right)^{\frac{1}{2}} - \left(1-D^2/4R^2\right)^{\frac{1}{2}}\right]}{\left[1-\left(n^2+1\right)D^2/4R^2\right]} \qquad \text{Equation A 4}$$

This last equation results from rationalizing the denominator of the previous. The equation for the limiting form of w(z), which becomes the ascending segment of a marginal ray, simplifies to

$$w(z) = D/2 + z \tan(A - B). \qquad \text{Equation A 5}$$

Thus, we have at twice the focal length from O, where for a thin lens z = R/(n – 1), the following

$$w(R/(n - 1)) = D/2 - (R/(n - 1))\tan(A - B). \qquad \text{Equation A 6}$$

As a consequence, we have for the maximum diameter of the SLM that would not suffer from a pupil restriction the following

$$d_{max} = D\{1 - [n(1 - n^2D^2/4R^2)^{1/2} - (1 - D^2/4R^2)^{1/2}] / (n - 1)[1 - (n^2 + 1)D^2/4R^2]\}.$$

Equation A 7

For a reasonable notional example where R = 15 cm, D = 3 cm, and n = 1.6, we get a value of 1.432 cm for d_{max}. For an SLM of 256 × 256 pixels and a pitch of 20 μm (or 0.002 cm), we have for the diagonal length of the active field 0.724 cm, which is slightly more than half of d_{max}. Thus, we can expect no influence of the pupil size for dimensions approximately the same as these. Examination of the situation for a plano-convex lens led to extensive algebraic manipulations because of the lack of symmetry; therefore, this investigation was discontinued. However, it is expected that the completed examination would lead to similar results for similar parameters for the items employed.

APPENDIX B — Aberration Error Due to a Spherical Lens in a Pixel-to-Pixel Case

Only ray tracing with Snell's law for refraction and geometric (actually trigonometric) consideration is employed in deriving the formulas for transverse deviations of the rays due to aberration. Symbols used are apparent in their definitions from their appearance as labels in Figure B1, Figure B2, and Figure B3 whose lens representations are exaggeratedly thick for ease of depiction and labeling. The z-axis of the rectangular coordinates used coincides with the optical axis of the lenses; the x- and y-axes are perpendicular to the optical axis; the symbol $w = (x^2 + y^2)^{1/2}$ denotes the distance from the optical axis; values of h, the distance from the optical axis at which the incident rays meet the lenses, are particular values of w. The origin on the axis will vary according to the convenience best suited for each lens example.

First, we consider the case of the doubly convex lens — a doubly convex lens will have the most involved derivation. The incident ray is refracted entering the lens at P, whose coordinates are $(2R - T - (R^2 - h^2)^{1/2}, h)$, where T is the lens' thickness and equal to $2(R - (R^2 - D^2/4)^{1/2})$.

From this, the coordinates of P are $(2R - 2(R^2 - D^2/4)^{1/2} - (R^2 - h^2)^{1/2}, h)$. The ray is again refracted as it emerges from the lens at Q, whose coordinates are $((R^2 - k^2)^{1/2}, k)$, where k is to be determined. We seek an equation for the ray emerging from the lens at Q. The symbols used are defined by their appearance on Figure B1.

To determine k, from Figure B1, we have

$$h - k = [(R^2 - k^2)^{1/2} + (R^2 - h^2)^{1/2} - 2(R^2 - D^2/4)^{1/2}] \tan(\theta_1-\theta_2). \quad \text{Equation B 1}$$

Abbreviating by defining

$$A = (2(R^2 - D^2/4)^{1/2} - (R^2 - h^2)^{1/2})\sin(\theta_1-\theta_2) + h\cos(\theta_1-\theta_2), \quad \text{Equation B 2}$$

we have

$$(R^2 - k^2)^{1/2}\sin(\theta_1-\theta_2) = A - k\cos(\theta_1-\theta_2). \quad \text{Equation B 3}$$

We square and rearrange terms in the resulting equation to get a quadratic equation for k, as follows

$$k^2 - 2kA\cos(\theta_1-\theta_2) + A^2 - R^2\sin(\theta_1-\theta_2) = 0. \quad \text{Equation B 4}$$

Solving, we have

$$k = A\cos(\theta_1-\theta_2) - (R^2 - A^2)^{1/2}\sin(\theta_1-\theta_2), \quad \text{Equation B 5}$$

where we have chosen the negative sign for the square root in order for $\cos\theta_3$ to be a positive quantity. We note that θ_3 is the acute angle between the line containing the ray segment from P to Q and the line containing the normal to the lens at Q, its cosine being given by the inner product (dot product) of the two-unit, normalized-coefficient vectors associated with these two lines. An equation for the line through P and Q is

$$- z \tan(\theta_1-\theta_2) - w + (2R - 2(R^2 - D^2/4)^{1/2} - (R^2 - h^2)^{1/2})\tan(\theta_1-\theta_2) + h = 0.$$

Equation B 6

An equation for the line containing the normal to the lens at Q (i. e., containing O and Q) is

$$k z - w (R^2 - k^2)^{1/2} = 0. \quad \text{Equation B 7}$$

Therefore, with substitution of the expressions for $(R^2 - k^2)^{1/2}$ and k from above and with the abbreviation A, we have

$$\cos\theta_3 = ((R^2 - k^2)^{1/2}\cos(\theta_1-\theta_2) - k \sin(\theta_1-\theta_2)) / R = (R^2 - A^2)^{1/2}/R$$

Equation B 8

and

$$\sin\theta_3 = A/R. \qquad \text{Equation B 9}$$

As one can see from Figure B1, the slope of the line containing the emergent ray at Q is $-\tan(\theta_4-\theta_5)$. However, again from the figure and from geometric considerations, $\theta_5+\theta_1 = \theta_3+\theta_2$ or $\theta_5 = \theta_3 + \theta_2-\theta_1$. Hence,

$$\tan(\theta_4-\theta_5) = [\tan(\theta_4-\theta_3) + \tan(\theta_1-\theta_2)] / [1 - \tan(\theta_4-\theta_3)\tan(\theta_1-\theta_2)].$$

Equation B 10

Therefore, with Snell's Law of Refraction, we have

$$\sin\theta_4 = n \sin\theta_3 = nA/R \qquad \text{Equation B 11}$$

and

$$\cos\theta_4 = (1 - n^2A^2/R^2)^{1/2}. \qquad \text{Equation B 12}$$

We also have

$$\sin(\theta_1-\theta_2) = (h/R)((1 - h^2/n^2R^2)^{1/2} - (1/n)(1 - h^2/R^2)^{1/2}) \qquad \text{Equation B 13}$$

and

$$\cos(\theta_1-\theta_2) = (1 - h^2/R^2)^{1/2}(1 - h^2/n^2R^2)^{1/2} + h^2/nR^2. \qquad \text{Equation B 14}$$

This enables us to rewrite A in terms of the given quantities, R, h, and n, as follows

$$A = h [(2(1 - D^2/4R^2)^{1/2} ((1 - h^2/n^2R^2)^{1/2} - (1/n)(1 - h^2/R^2)^{1/2}) +1/n].$$

Equation B 15

We can also define k as

$$k = A((1 - h^2/R^2)^{1/2}(1 - h^2/n^2R^2)^{1/2} + h^2/nR^2)$$

$$- h(1 - A^2/R^2)^{1/2}((1 - h^2/n^2R^2)^{1/2} - (1/n)(1 - h^2/R^2)^{1/2})).$$

Equation B 16

Furthermore, using the above trigonometric equations relating θ_4 and θ_3 to A, R, and n, we get

$$\tan(\theta_4 - \theta_3) = \frac{A\left[n\left(1 - A^2/R^2\right)^{\frac{1}{2}} - \left(1 - A^2/n^2R^2\right)^{\frac{1}{2}}\right]}{\left[R\left(1 - A^2/R^2\right)^{\frac{1}{2}}\left(1 - n^2A^2/R^2\right)^{\frac{1}{2}} + nA^2/R^2\right]}$$

$$= A[n(1 - n^2A^2/R^2)^{1/2} - (1 - A^2/R^2)^{1/2})] /R\,[1 - (n^2+1)A^2/R^2].$$

Equation B 17

where the latter equation is obtained by rationalizing the denominator of the former. Similar manipulations using the above trigonometric equations relating θ_1-θ_2 to h, R, and n yield

$$\tan(\theta_1 - \theta_2) = \frac{h\left[n\left(1 - h^2/n^2R^2\right)^{\frac{1}{2}} - \left(1 - h^2/R^2\right)^{\frac{1}{2}}\right]}{R\left[n\left(1 - h^2/n^2R^2\right)^{\frac{1}{2}}\left(1 - h^2/R^2\right)^{\frac{1}{2}} + h^2/R^2\right]}$$

$$= \frac{h\left[\left(1 - h^2/R^2\right)^{\frac{1}{2}} - (1/n)\left(1 - h^2/n^2R^2\right)\right]}{R\left[1 - \left(n^2 + 1\right)h^2/n^2R^2\right]}$$

Equation B 18

where again we rationalized the denominator.

These two tangent relations enable one to evaluate, in terms of the given quantities, the slope, $-\tan(\theta_4-\theta_5)$, of the line containing the emergent ray at Q, as follows

$$w = k - (z - (R^2 - k^2)^{1/2})\tan(\theta_4-\theta_5). \qquad \text{Equation B 19}$$

In particular, to estimate the resultant aberration, we are interested in the value of w for z at the focus of the lens, $z = R((1 - D^2/4R^2)^{1/2} + 1/(n - 1))$, and at twice the focal length away from the lens' optical center, where $x = R((1 - D^2/4R^2)^{1/2} + 2/(n-1))$.

Next, in decreasing order of complexity, we deal with the case of the plano-convex lens with the ray incident on the spherical face. Again, the ray enters the lens at P, whose coordinates are $(R - (R^2 - h^2)^{1/2})$, h), is refracted, and emerges, refracted again, from the lens at Q, whose coordinates are $(R - (R^2 - D^2/4)^{1/2}$, k), where k is to be determined. We seek relations in terms of given R, h, and n for the values of k and $\tan\theta_4$ in the equation for the line containing the ray emergent at Q, as follows

$$w = k - (z - R + (R^2 - D^2/4)^{1/2})\tan\theta_4. \qquad \text{Equation B 20}$$

We are particularly interested in the values of w for $w = R/(n -1)$ (i. e., at the lens focus) and at $w = 2R/(n - 1)$ (i. e., at twice the focal distance).

To determine k, from geometric considerations and noting from Figure 2 that $\theta_3 = \theta_1-\theta_2$, we have

$$h - k = ((R^2 - h^2)^{1/2} - (R^2 - D^2/4)^{1/2})\tan\theta_3 \qquad \text{Equation B 21}$$

that is,

$$k = h - R((1 - h^2/R^2)^{1/2} - (1 - D^2/4R^2)^{1/2})\tan(\theta_1-\theta_2) \qquad \text{Equation B 22}$$

Next, we seek the slope, $-\tan\theta_4$, of the line containing the emergent ray from Q. From Figure B2, we see that the angle $\theta_3 = \theta_1 - \theta_2$. Consequently, with Snell's law, $\sin\theta_1 = n\sin\theta_2$ and $\sin\theta_4 = n\sin\theta_3$ and with $\sin\theta_1 = h/R$, we have

$$\tan\theta_4 = n\sin\theta_3/(1 - n^2\sin^2\theta_3)^{1/2} = n\sin(\theta_1-\theta_2)/(1 - n^2\sin^2(\theta_1-\theta_2))^{1/2},$$

Equation B 23

where, as derived earlier in the case of the doubly convex lens in terms of given R and h,

$$\sin(\theta_1-\theta_2) = (h/R)((1 - h^2/n^2R^2)^{1/2} - (1/n)(1 - h^2/R^2)^{1/2}))$$ Equation B 24

and

$$\cos(\theta_1-\theta_2) = (1 - h^2/n^2R^2)^{1/2}(1 - h^2/R^2)^{1/2}) + h^2/nR^2.$$ Equation B 25

Therefore, at the focus, where $z = R/(n - 1)$, we have

$$w = w_1 = h - R(1 - h^2/R^2)^{1/2} - (1 - D^2/4R^2)^{1/2})\tan(\theta_1-\theta_2)$$
$$- R((2 - n)/(n - 1) + (1 - D^2/4R^2)^{1/2})\tan\theta_4.$$ Equation B 26

At a disance of twice the focal length, where $z = 2R/(n - 1)$, we have

$$w = w_2 = h - R(1 - h^2/R^2)^{1/2} - (1 - D^2/4R^2)^{1/2})\tan(\theta_1-\theta_2)$$
$$- R((3 - n)/(n - 1) + (1 - D^2/4R^2)^{1/2})\tan\theta_4,$$ Equation B 27

formulas from which by direct calculations, one obtains numerical values for the desired quantities, given values of the parameters, R, D, h, and n.

Finally, we examine the simplest case of the three: a plano-convex lens with the ray incident on the plane face. The ray is not refracted until it reaches the exit point, Q, from the lens. The coordinates of Q are $((R^2 - h^2)^{1/2}, h)$. Referring to the Figure B3, we see that we seek a relation in terms of the given R, h, and n for the slope, $\tan(\theta_1-\theta_2)$, of the line for the emergent ray, as follows

$$w = h - (z - (R^2 - h^2)^{1/2})\tan(\theta_2-\theta_1). \qquad \text{Equation B 28}$$

Again, with the Snell' law relation, $\sin\theta_2 = n\sin\theta_1$, $\sin\theta_1 = h/R$, standard trigonometric relations, and a rationalization of a denominator, we have

$$\tan(\theta_2-\theta_1) = (h/R)[n(1 - h^2/R^2)^{1/2} - (1 - n^2 h^2/R^2)^{1/2}]$$
$$/[(1 - n^2h^2/R^2)^{1/2})\,(1 - h^2/R^2)^{1/2}) + nh^2/R^2]$$
$$= (h/R)[n(1 - n^2 h^2/R^2)^{1/2} - (1 - h^2/R^2)^{1/2})]/[1 - (n^2 + 1)h^2/R^2].$$

Equation B 29

At the lens focal point

$$z = R + R/(n-1) = nR/(n - 1) \qquad \text{Equation B 30}$$

and

$$w = w_1 = h - \frac{R\left[n/(n-1) - \left(1 - h^2R^2\right)^{\frac{1}{2}}\right](h/R)\left[n\left(1 - n^2h^2R^2\right)^{\frac{1}{2}} - \left(1 - h^2R^2\right)^{\frac{1}{2}}\right]}{1 - \left(n^2 + 1\right)\left(h^2/R^2\right)}$$

$$= \frac{h\left[1 - \left(n/(n-1) - \left(1 - h^2/R^2\right)^{\frac{1}{2}}\right)\left(n\left(1 - n^2\,h^2/R^2\right)^{\frac{1}{2}} - \left(1 - h^2/R^2\right)^{\frac{1}{2}}\right)\right]}{1 - \left(n^2 + 1\right)\left(h^2/R^2\right)}.$$

Equation B 31

At twice the focal distance

$$z = R + 2R/(n - 1) = (n + 1)R / (n - 1) \qquad \text{Equation B 32}$$

and

$$w = w_2 = h - \frac{R\left[(n+1)/(n-1) - \left(1-h^2R^2\right)^{\frac{1}{2}}\right](h/R)\left[n\left(1-n^2h^2R^2\right)^{\frac{1}{2}} - \left(1-h^2R^2\right)^{\frac{1}{2}}\right]}{1-\left(n^2+1\right)\left(h^2/R^2\right)}$$

$$= \frac{h\left[1-\left((n+1)/(n-1) - \left(1-h^2/R^2\right)^{\frac{1}{2}}\right)\left(n\left(1-n^2h^2/R^2\right)^{\frac{1}{2}} - \left(1-h^2/R^2\right)^{\frac{1}{2}}\right)\right]}{1-\left(n^2+1\right)\left(h^2/R^2\right)}.$$

Equation B 33

FIGURE CAPTIONS

Figure 1: Baseline parallel processor consists of three 3-port devices, two SLMs and one CCD for output.

Figure 2: A spatial light modulator representing a 256 X 256-bin register, with each bin capable of holding an 8-bit word.

Figure 3: Gaussian distribution of a two-state system containing two different expectation values, 0 and 1.

Figure 4: Probability of error plotted as a function of Q.

Figure 5: Aberration-induced displacement on a pixel.

Figure 6: Aperture determination setup.

Figure A.1: Schematic of ray P-Q-Q'-P' intersecting a lens at some distance, h, from its rim.

Figure B.1: Symmetric double-convex lens.

Figure B.2: Plano-convex lens with a ray incident on the convex face.

Figure B.3: Plano-convex lens with a ray incident on the planar face.

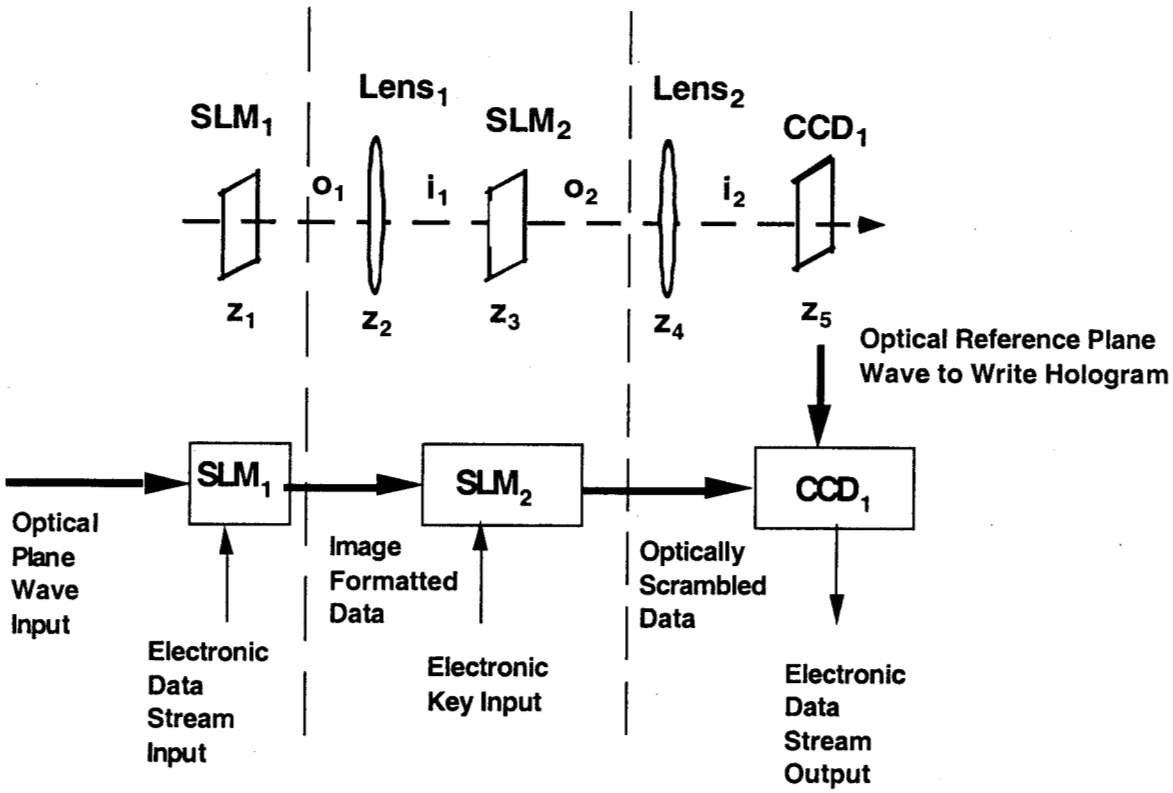
SLM1
Lens1
SLM2
Lens2
CCD1
o1
i1
o2
i2
z1
z2
z3
z4
z5
Optical Reference Plane
Wave to Write Hologram
SLM1
SLM2
CCD1
Optical
Plane
Wave
Input
Electronic
Data
Stream
Input
Image
Formatted
Data
Electronic
Key Input
Optically
Scrambled
Data
Electronic
Data
Stream
Output

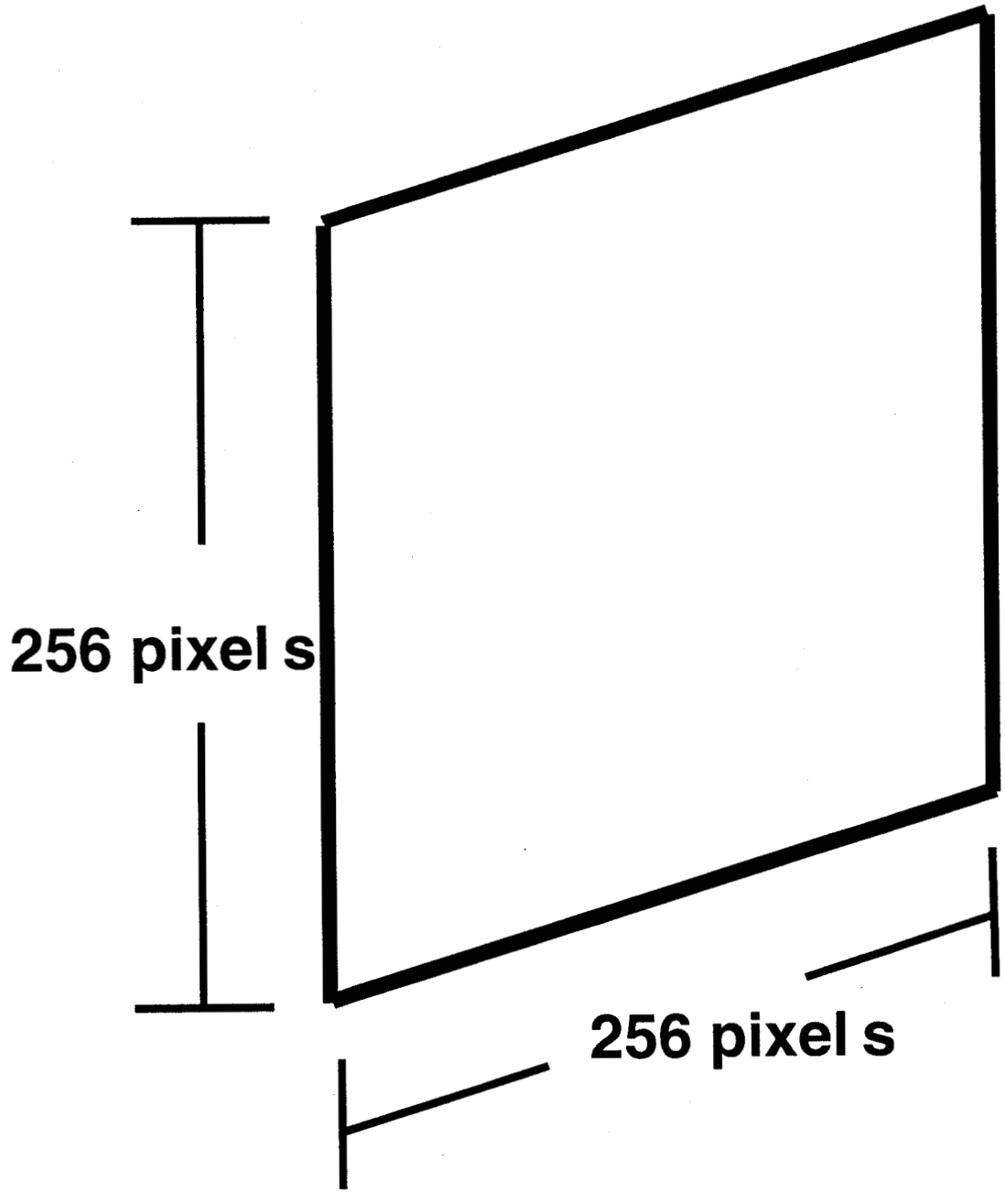
256 pixel s
256 pixel s

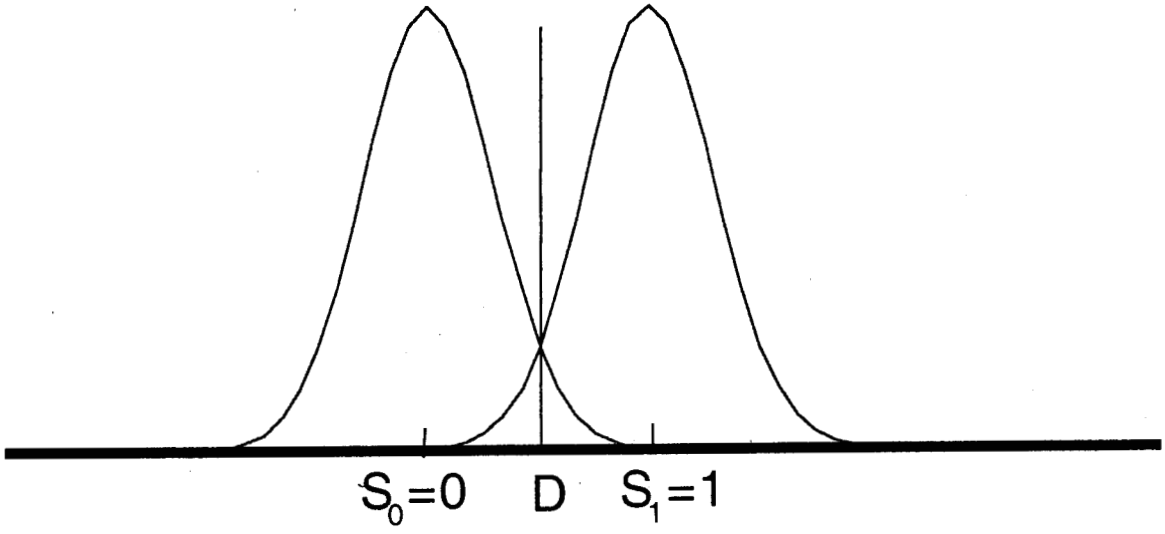
$S_0=0$
D
$S_1=1$

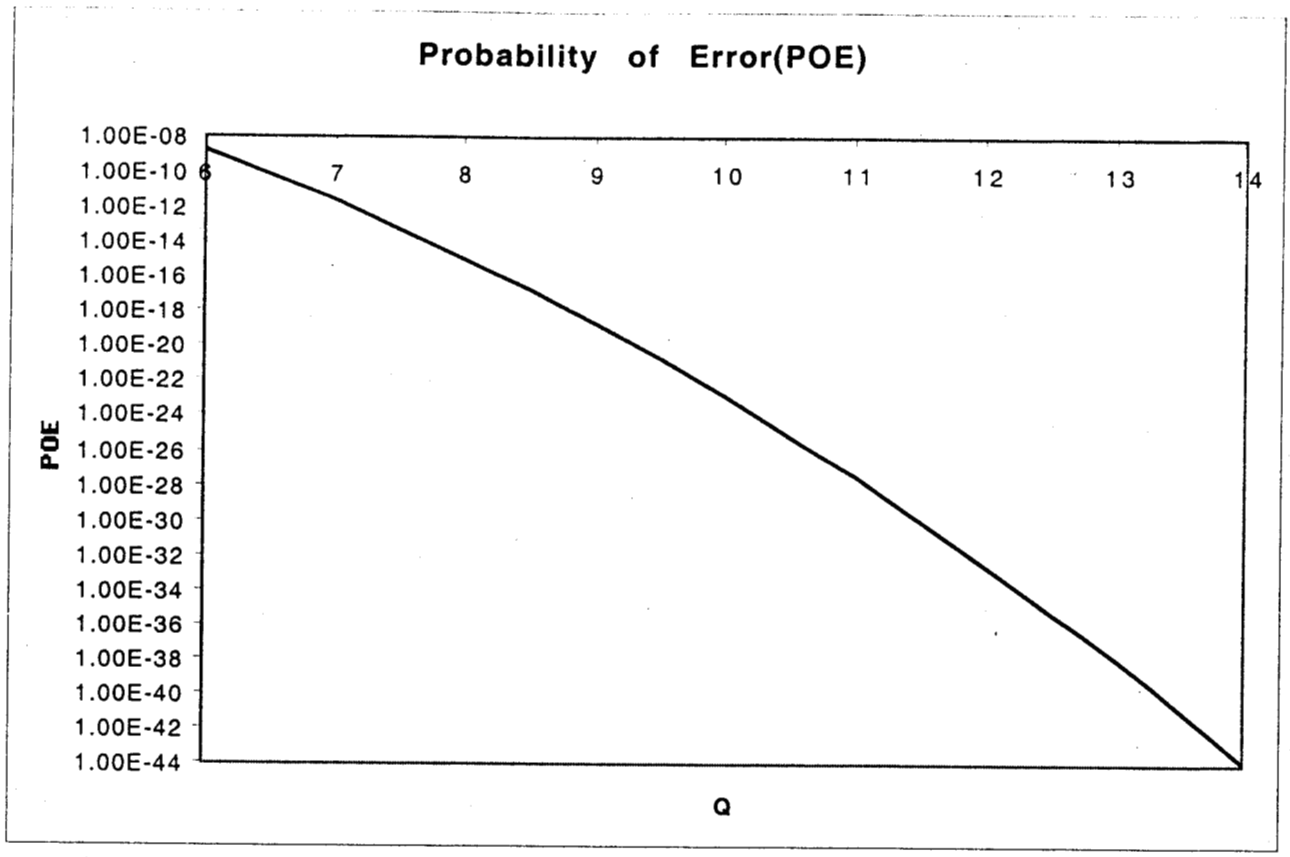
Probability of Error(POE)
POE
1.00E-08
1.00E-10
1.00E-12
1.00E-14
1.00E-16
1.00E-18
1.00E-20
1.00E-22
1.00E-24
1.00E-26
1.00E-28
1.00E-30
1.00E-32
1.00E-34
1.00E-36
1.00E-38
1.00E-40
1.00E-42
1.00E-44
6
7
8
9
10
11
12
13
14
Q

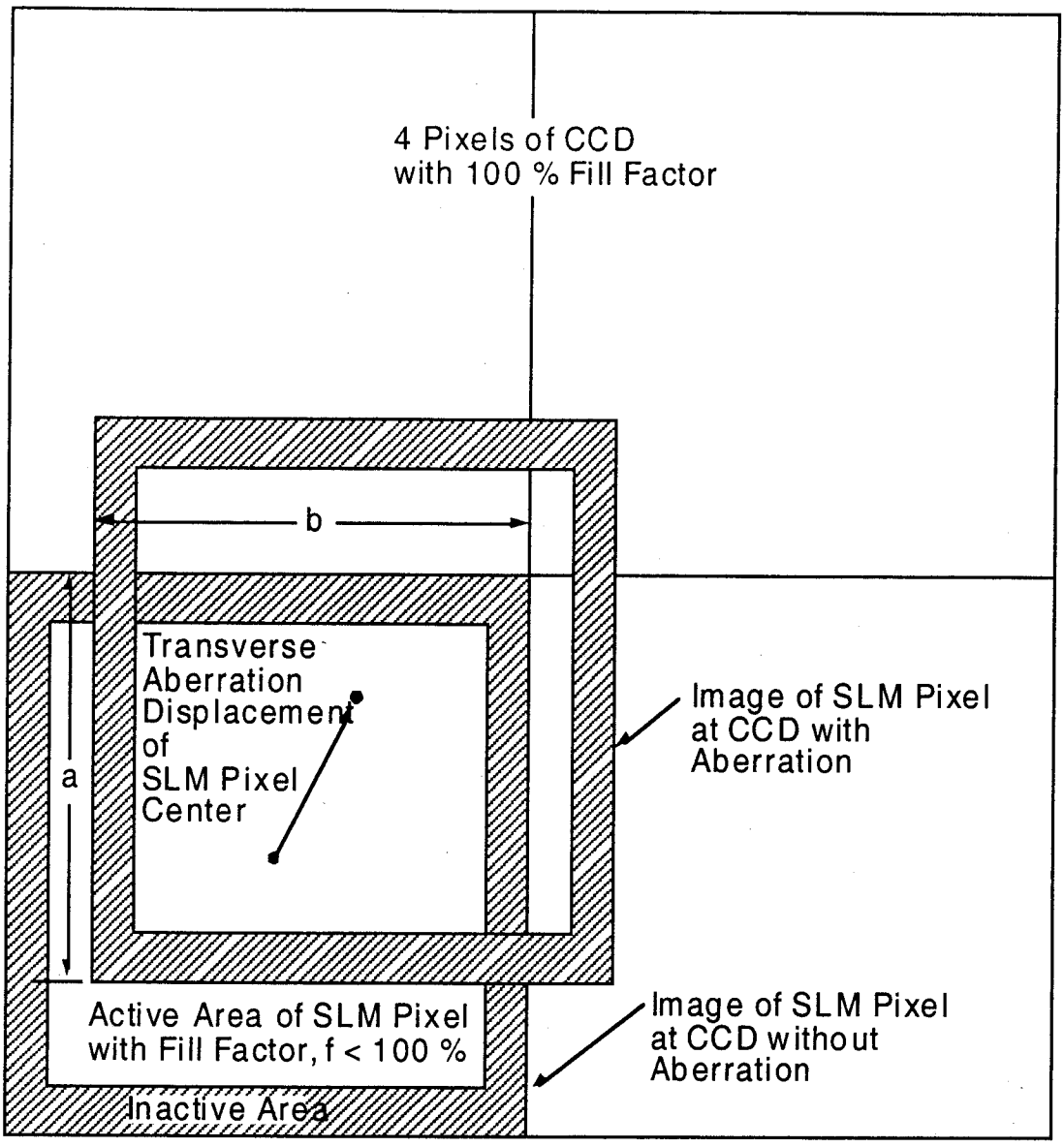
4 Pixels of CCD
with 100 % Fill Factor
b
a
Transverse
Aberration
Displacement
of
SLM Pixel
Center
Image of SLM Pixel
at CCD with
Aberration
Active Area of SLM Pixel
with Fill Factor, f < 100 %
Inactive Area
Image of SLM Pixel
at CCD without
Aberration

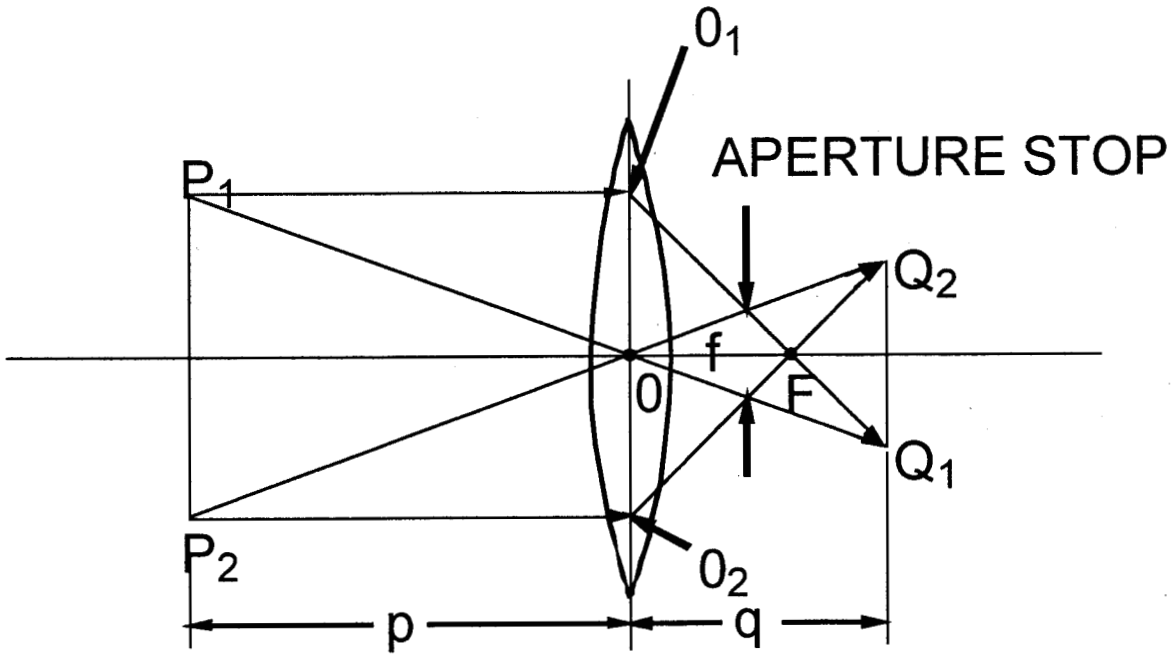
O_1
APERTURE STOP
P_1
Q_2
f
O
F
Q_1
P_2
O_2
p
q

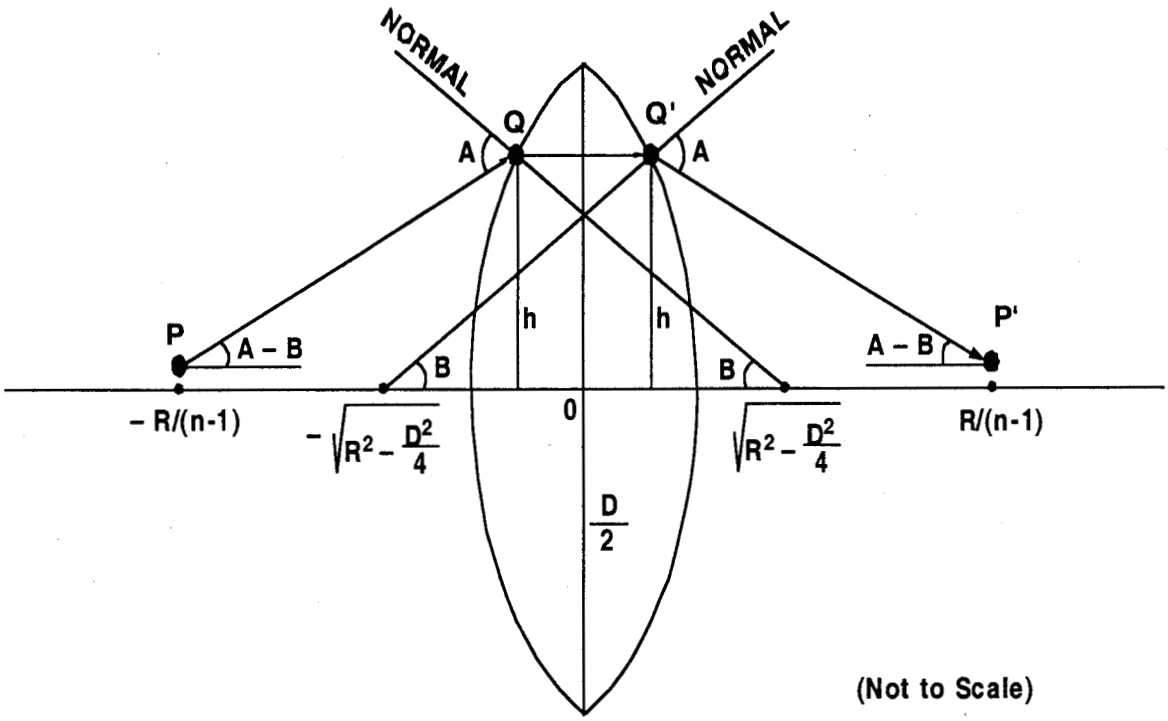
NORMAL
NORMAL
Q
Q'
A
A
P
A – B
A – B
P'
h
h
B
B
– R/(n-1)
$-\sqrt{R^2-\frac{D^2}{4}}$
0
$\sqrt{R^2-\frac{D^2}{4}}$
R/(n-1)
$\frac{D}{2}$
(Not to Scale)

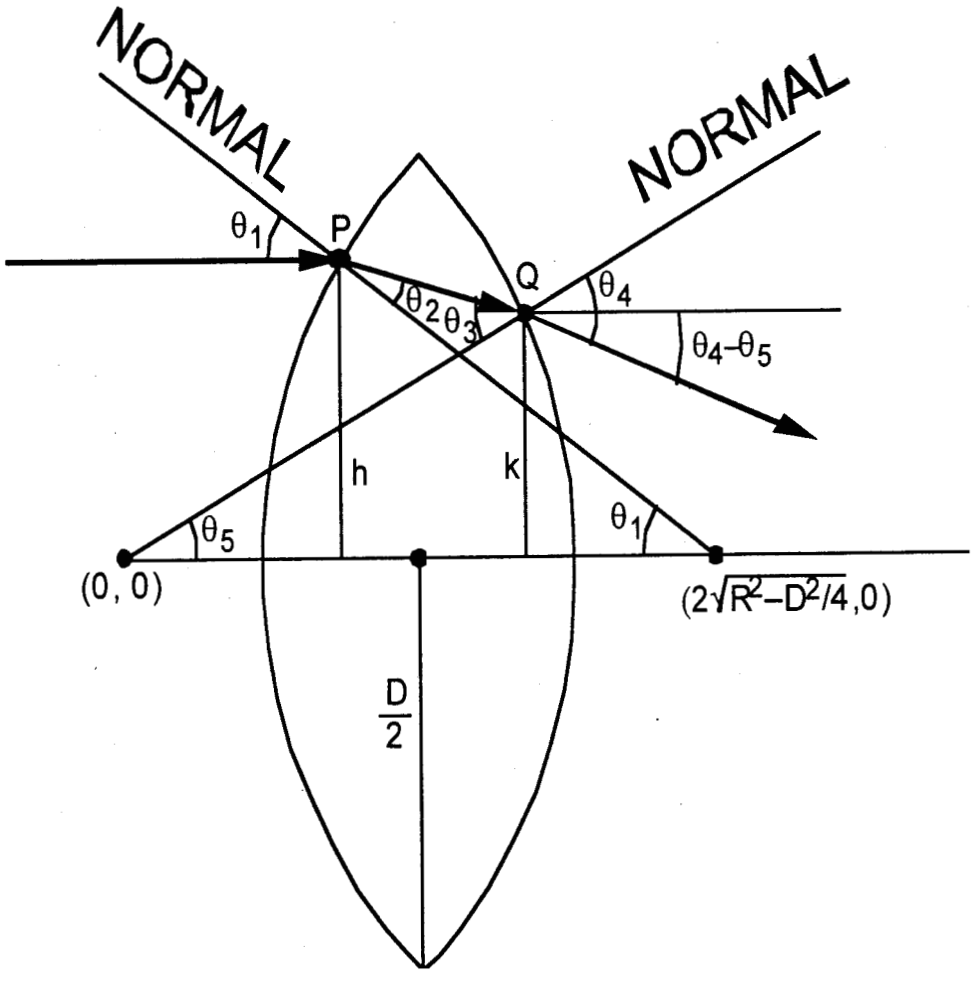
NORMAL
NORMAL
θ1
P
Q
θ2
θ3
θ4
θ4−θ5
h
k
θ5
θ1
(0, 0)
(2√R²−D²/4,0)
D/2

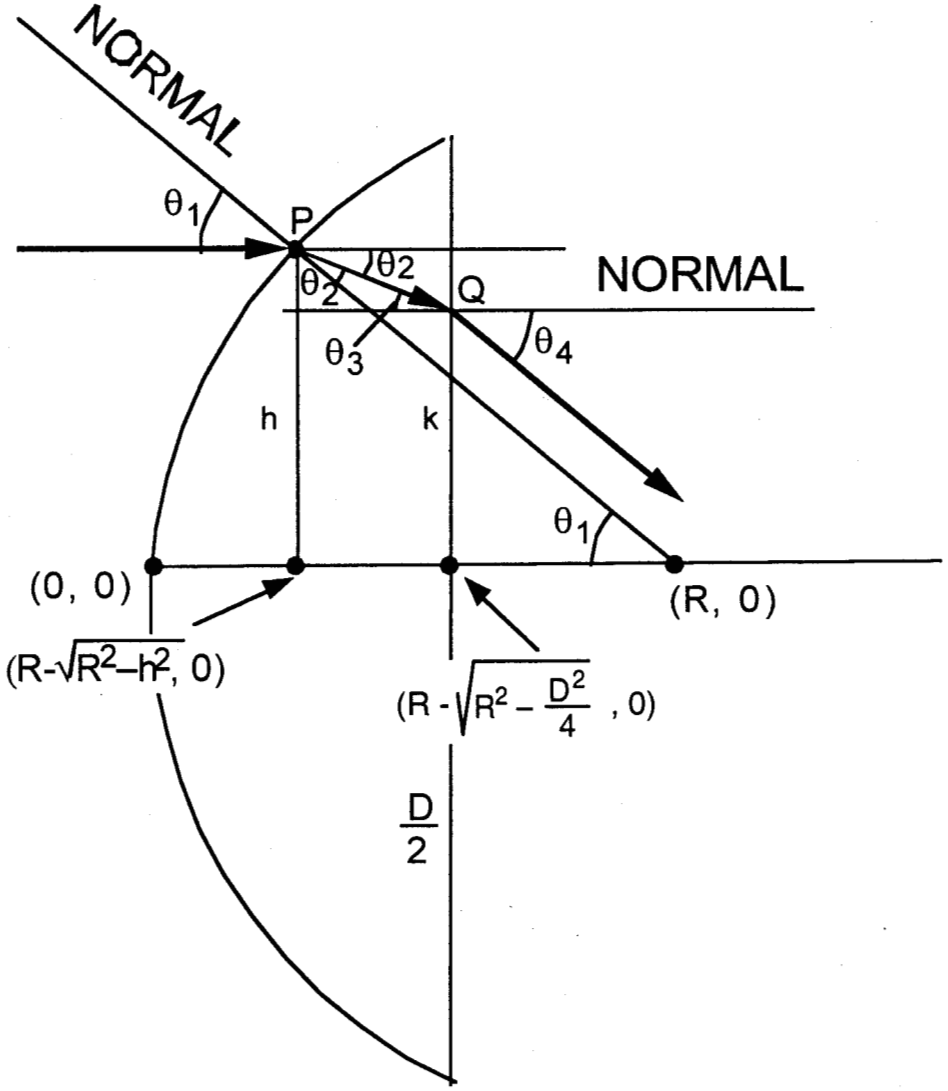
NORMAL
θ1
P
θ2
θ2
Q
NORMAL
θ3
θ4
h
k
θ1
(0, 0)
(R, 0)
(R-√R2–h2, 0)
(R - √R2 – D2/4 , 0)
D/2

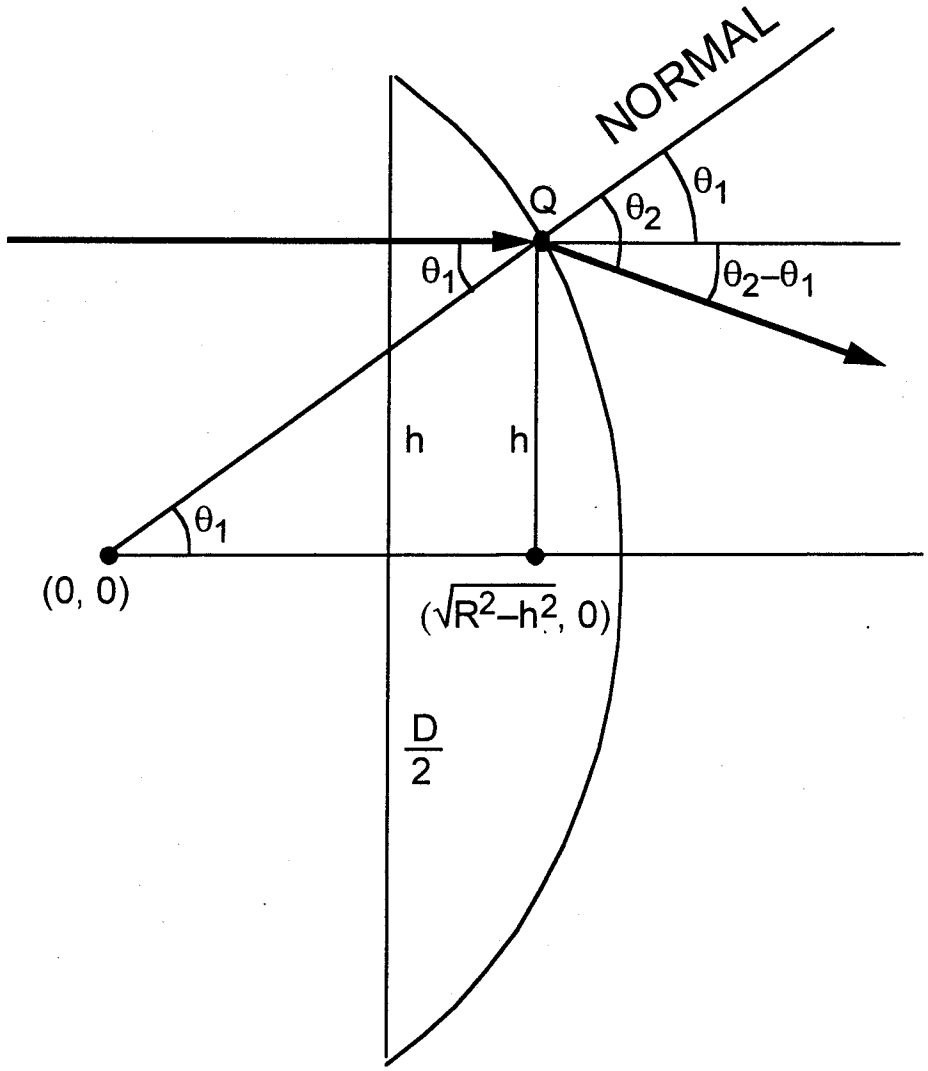
NORMAL
Q
θ2
θ1
θ1
θ2−θ1
h
h
θ1
(0, 0)
(√R2−h2, 0)
D
2

TABLE CAPTIONS

Table 1: Baseline processor design differences by application.

Table 2: Q, calculated as a function of the chosen n-bit grayscale for a setup where the SLM noise is negligible compared to the other noise terms.

Table 3: Offset aberration error due to lens (assuming a pixel pitch of 20 μm).

Table 4: Systematic error sources.

Application	Phase Modulation Input	Required BER
High Data Rate Routers	Holographic grating to reorder output rows from initial input order	10^{-9}
High Speed Encryption	Encryption key to scrambler phase	10^{-25}

n	I_{min} (current) (Amps)	Thermal noise ($Amps^2$)	Shot noise ($Amps^2$)	RIN Noise ($Amps^2$)	Q
1	4.10E-07	4.42E-20	2.83E-17	3.62E-21	77
2	2.05E-07	4.42E-20	1.42E-18	9.06E-22	54
3	9.11E-08	4.42E-20	6.30E-18	1.79E-23	36
4	4.28E-08	4.42E-20	2.96E-18	3.96E-23	25
5	2.07E-08	4.42E-20	1.43E-19	9.30E-24	17
6	1.02E-08	4.42E-20	7.06E-19	2.25E-25	12
7	5.07E-09	4.42E-20	3.50E-19	5.54E-25	8
8	2.52E-09	4.42E-20	1.74E-19	1.38E-25	5

Lens Type	Transverse Aberration at Focus (μm)	Transverse Aberration at Twice Focus (μm)
Symmetric Double Convex	15 (~3/4 pitch length)	17.3 (~7/8 pitch length)
Plano-Convex (Incident on convex face)	3.4 (~1/6 pitch length)	-2.4 (~1/8 pitch length)
Plano-Convex (Incident on planar-face)	2.7 (~1/7 pitch length)	4.7 (~1/4 pitch length)

Error Source	Magnitude of Error	Comments
Error due to finite size of lens pupil	Negligible	Assumes lens diameter several times SLM, CCD diagonal dimensions
Aperture stops	Potentially negligible	Assumes optimum positioning of aperture
Aberration error due to lens in Pixel-to-pixel transforms	Varies with each pixel	Interacts with fill factor
Error due to fill factor of SLM		Interacts with and can be used to compensate for lens aberration
Electro-Optical conversion sffect at the SLM	May vary with each pixel	Can be compensated through calibration
Noise due to Stray Light sources	Likely largest systematic source	Spatial hot spots; aperture stops and high quality optical elements reduce impact